CHAPTER 5

DESIGN AND DEVELOPMENT OF FILLETED RECTANGULAR DIELECTRIC RESONATOR ANTENNA USING PBBS GLASS ADDED BST (BST-3P)

5.1 Introduction

Now-a-days, radar and satellite communication demand wide bandwidth for effective performance. Wideband signal can provide high data rate, multiple audio and video channels simultaneously and it can help in determining range or depth of a target with high accuracy. Hence, for such applications large impedance bandwidth of more than 50% is required through single antenna. The dielectric resonator antenna (DRA) is a structure where dielectric opens in free space to resonate and radiate due to explicit symmetry breaking [Sinha et al. (2015)]. These DRAs can provide wide impedance bandwidth and are good candidates for aforesaid applications. DRA materials possess low dielectric loss and zero conductor loss. They have several advantages, such as size control through change in dielectric, wide bandwidth, commonly broadside radiation pattern and flexibility to various feed arrangements. Wide bandwidth of DRA can be achieved by stacking multi-permittivity DRAs, modifying the shape of DRA, using different types of feeding structures, etc. Among different shapes of DRA, rectangular shaped DRA possesses more flexibility as it has two degrees of freedom and is easy to shape manually. Lower dielectric constant of DRA can provide large bandwidth but it will increase the antenna size for a given frequency. Further, tendency of the field to emerge from the DRA material will increase for lower dielectric constant, which would affect occurrence of resonance in the DRA. High dielectric constant and low loss tangent DRA material

supports efficient coupling of electromagnetic signal through different feed structures, high radiation efficiency and antenna miniaturization.

In recent years, the engineers/scientists working in electronic industries started taking keen interest in barium strontium titanate (BST) because of its relatively high dielectric constant, low loss, greater breakdown field strength and good mechanical and thermal properties. Due to ferroelectric and dielectric nature of BST, it is used as leading material for design of several microwave components / antennas, at microwave frequencies such as phase shifters, oscillators, tunable filters, dielectric resonator antennas etc. [Brankovic et al. (2005)]. Barium strontium titanate (BST) with high dielectric constant also has the property of standing wave (resonance frequency) formation inside the material at microwave frequencies. Due to this property of BST, it became potential dielectric material for dielectric resonator antennas (DRA) [Ullah et al. (2015)]. Higher dielectric constant material provides sufficient electromagnetic coupling to the excitation source and makes the antenna size smaller at a given frequency.

In the present chapter, 3wt% PBBS glass added BST named as BST-3P, was used as a resonating segment for antenna designs. It provides material dielectric constant of 15, which is required for the design of proposed antenna under investigation in this chapter. The synthesis and characterisation of BST-3P ceramic is described thoroughly in chapters 3 and 4, respectively. The simulation studies of single segment rectangular DRA (SS-RDRA), double segment rectangular DRA (DS-RDRA) and filleted rectangular DRA (F-RDRA) were carried out using Ansys HFSS software at microwave frequencies and simulation results for input and / or radiation characteristics are compared. The proposed filleted RDRA (F-RDRA) was fabricated (fabrication steps described in section 3.4.2(a) in chapter 3) and measurements were performed. The simulation results for input and

radiation characteristics of the proposed F-RDRA are compared with respective experimental results as well as with the results for conventional dual segment RDRA (DS-RDRA). Further, the input characteristics of the proposed F-RDRA are also compared with those of RDRAs reported in the literature.

5.2 Antenna Design and Discussion

Small size, low profile and simple antenna structure with ease of fabrication, low production cost (when commercially produced) and good antenna performance including wideband performance are certain factors, which should be considered during the design of a practical antenna. Although, various complex DRAs have been studied and found to give good performance, yet they are not utilized practically due to the absence of one of the afore-mentioned characteristics. Different bandwidth enhancement techniques, such as optimization of DRA parameters, feeding mechanisms, DRA stacking, structural modification in DRA are used for design of practical RDRAs.

5.2.1 Feeding mechanism

Various feeding mechanisms, such as microstrip feed, coaxial probe feed, aperture coupling and proximity feed have been studied for the excitation of DRAs. In microstrip line and coaxial feeds, there is a drawback of spurious feed radiation generated and the bandwidth obtained with impedance matching is also less when compared with the aperture coupling and proximity feed. Out of these feeds, proximity feed provides the widest bandwidth. In terms of ease of fabrication, proximity feed is quite complex to design. Therefore, aperture-coupled feed is selected as feed for the proposed F-RDRA which can provide good impedance bandwidth with less spurious feed radiation and moderate ease of fabrication [Luk and Leung (2003); Petosa (2007)]. The optimized

geometrical parameters of the proposed aperture-coupled antenna and material dielectric constants are given in Table 5.1.

5.2.2 Stacking of resonating elements

Stacking of different resonating elements having different permittivities provides enhanced bandwidth due to coupling of radiation from the lower permittivity resonator acting as lower segment to higher permittivity resonator element acting as upper segment of the antenna. The low permittivity insert in the design of antenna completely separates the high permittivity dielectric resonator from the ground plane, forcing all the electric field lines of force to pass through the low permittivity region [Gupta and Gangwar (2016)]. Therefore, bandwidth gets enhanced when the low permittivity resonator element is kept as lower resonating segment and the high permittivity resonator element as the upper segment in the stack. Various dual segment or multi segment DRAs with resonating elements of different permittivities have been studied to achieve wide impedance bandwidth [Soren et al. (2014), Kumari and Gangwar (2016)]. In the present study, Teflon of $\varepsilon_r = 2.1$ is used as lower segment while BST-3P ceramic of average $\varepsilon_r = 15$ is used as upper segment of the proposed antenna.

5.2.3 Structural novelty in DRA

The simulation study of a simple single segment RDRA (SS-RDRA) (made of BST-3P) and a conventional dual segment RDRA (DS-RDRA) with microstrip line fed aperture coupling was carried out using Ansys HFSS software. Optimized geometrical parameters of the two antennas and material dielectric constants are given in Table 5.1. Input reflection coefficient–frequency characteristics of the afore-mentioned antennas were simulated using Ansys HFSS software and simulation results are shown in figure 5.3(a).

The conventional DS-RDRA provides enhanced bandwidth as compared with SS-RDRA (Figure 5.3(a) and Table 5.2). In order to achieve further improvement in bandwidth of conventional DS–RDRA, the upper edges in the broad dimension of upper segment (made of BST-3P) were made filleted in the DS-RDRA (named as Filleted–RDRA). Simulated input characteristics of the antenna are extracted from figure 5.3(a) and the simulation results are given in Table 5.2. The optimized filleted radius of the proposed antenna is given in Table 5.1. It is found through simulation and experimental studies that the proposed F-RDRA gives higher bandwidth with insignificant reduction in gain as compared with conventional DS-RDRA. Figures 5.1(a) and 5.2(a) show the 3-D views of conventional DS-RDRA and the proposed F-RDRA respectively. A design approach for the proposed F-RDRA has been successfully demonstrated to achieve enhanced bandwidth and good gain over its operating frequency range, in X– or Ku– bands.

5.2.4 Theoretical analysis of antenna design

Resonant frequency (f_o) is defined as

$$f_o = \frac{Fc}{2\pi L_d \sqrt{\varepsilon_r}}, \tag{5.1}$$

where F is normalised frequency, c is velocity of light, L_d is length of RDRA and ε_r is effective permittivity of the stacked RDRA. Normalised frequency value can be observed from the standard graph of normalised frequency versus ratio of DRA dimensions (W_d/b) for various ratio of L_d/b.

Effective permittivity (ε_r) of the stacked RDRA can be calculated using

$$\varepsilon_r = \frac{H_{eff}}{\frac{d}{\varepsilon_u}+\frac{t}{\varepsilon_l}}, \tag{5.2}$$

where H_{eff} (effective height) = d+t, h is height of upper segment, t is height of lower segment, ε_u is permittivity of upper segment and ε_l is permittivity of lower segment.

Resonant frequencies of 10.88 GHz and 12.22 GHz in case of DS-RDRA and F-RDRA respectively were obtained from the above mentioned equation by taking the values of parameters from Table 5.4. The values of resonant frequencies are very close to those obtained through simulation and measurement. Differences in calculated, simulated and measured resonant frequencies may be due to aperture loading of RDRA.

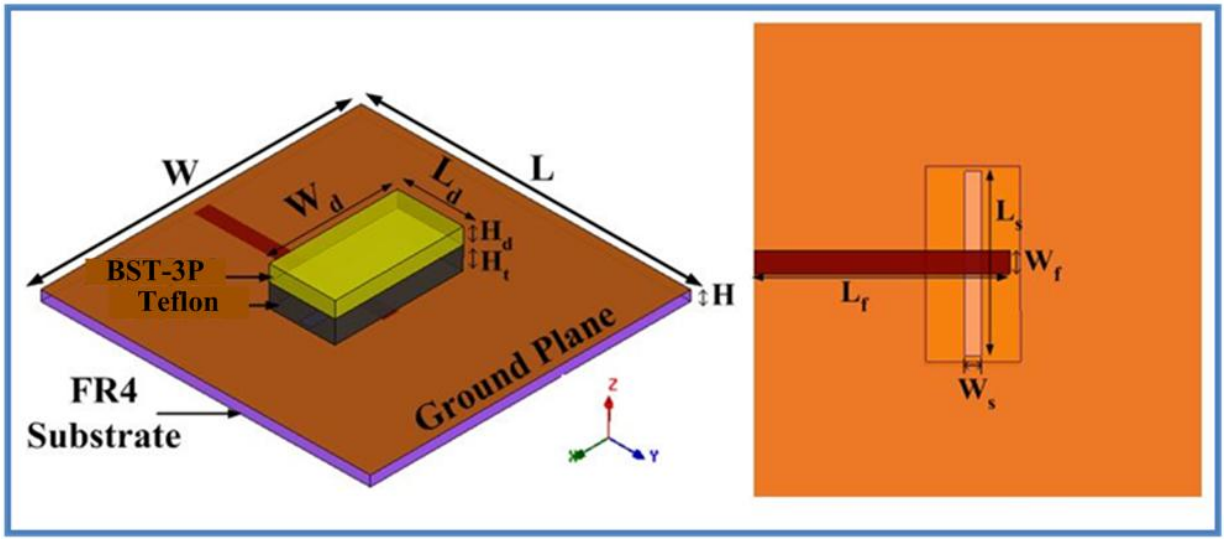

Figure 5.1 Geometry of DS-RDRA (a) 3-D view, (b) bottom view.

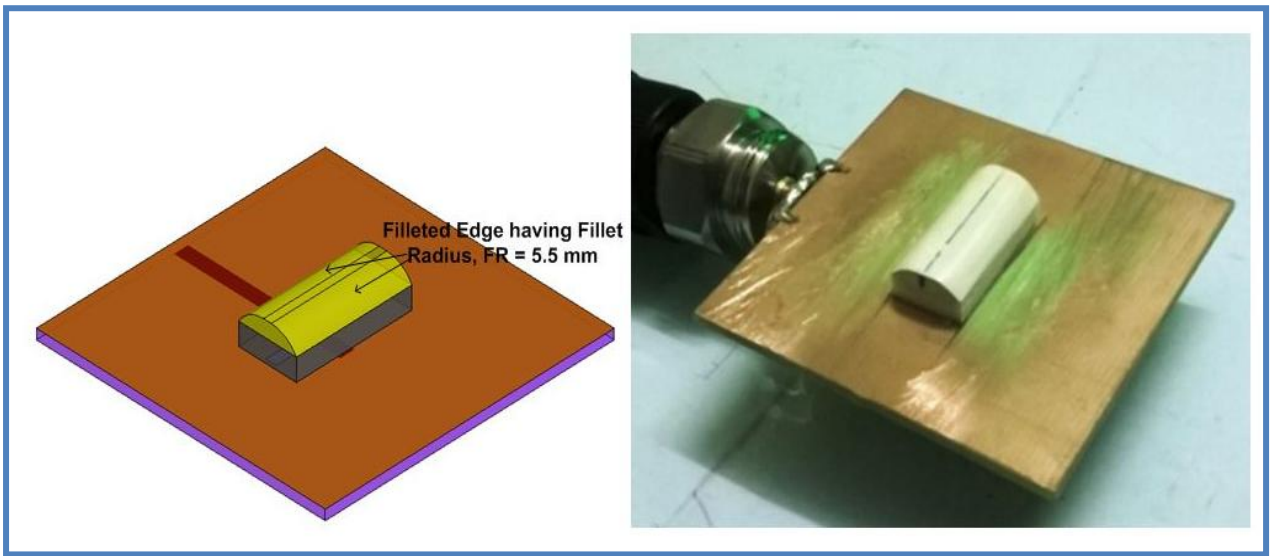

Figure 5.2 Geometry of F-RDRA (a) 3-D view, (b) Fabricated F-RDRA

Table 5.1 Parameters of SS-RDRA, DS-RDRA and proposed F-RDRA.

Antenna Parameter	Value
Substrate dimension (L × W × H)	50 mm × 50 mm × 1.6 mm
*Dimension of upper segment ($L_d \times W_d \times H_d$)	10 mm× 20 mm × 2.5 mm
*Dimension of lower segment ($L_d \times W_d \times H_t$)	10 mm× 20 mm × 3.5 mm
**Dimension of single segment ($L_d \times W_d \times H_s$)	10 mm× 20 mm × 2.5 mm
Feedline dimensions($L_f \times W_f$)	28.9 mm × 2.5 mm
Slot dimensions ($L_s \times W_s$)	18.9 mm × 1.8 mm
Fillet Radius (FR)	5.5 mm
Dielectric constant of prepared dielectric	15
Dielectric constant of Teflon	2.1

*for DS-RDRA and F-RDRA; **for SS-RDRA.

5.3 Results and Discussion

5.3.1 Reflection coefficient – frequency characteristics

Figure 5.3(a) shows the simulated variations of reflection coefficient of SS-DRDRA, conventional DS-RDRA and proposed F-RDRA versus frequency. Figure 5.3(a) represents that -10 dB reflection coefficient bandwidth of conventional DS-RDRA is 3.65 GHz (39.35 %) which is much larger than the bandwidth of SS-RDRA (0.17 GHz) (1.5%). The -10 dB reflection coefficient bandwidth of F-RDRA is increased by 8.57% when compared with conventional DS-RDRA. This may be due to less dielectric loss in case of F-RDRA due to less dielectric volume covered as compared with conventional DS-RDRA.

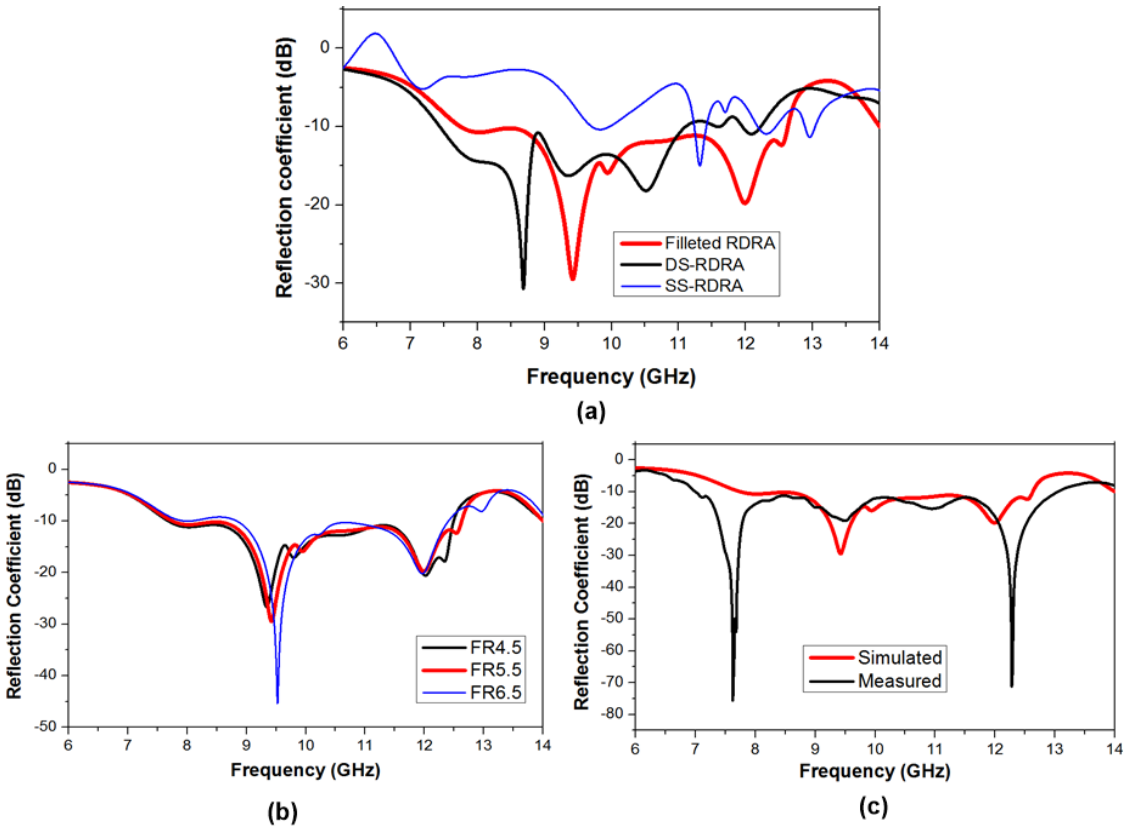

Figure 5.3 (a) Simulated variations of reflection coefficient of SS-RDRA, DS-RDRA and the proposed F-RDRA versus frequency; (b) Effect of variation in fillet radius over the range 4.5 - 6.5 mm on the reflection coefficient of F-RDRA and (c) Simulated and measured variations of reflection coefficient of F-RDRA with frequency.

Table 5.2 Reflection coefficient–frequency characteristics of SS-RDRA, conventional DS-RDRA and F-RDRA.

DRA Shape	**Resonant Frequency**	**Operating Frequency Range (GHz)**	**-10 dB reflection coefficient Bandwidth (%)**
Simulated SS-RDRA	11.32 GHz	0.17 GHz (11.24 – 11.41 GHz)	1.5
Simulated DS-RDRA	8.68 GHz 10.52 GHz	3.65 GHz (7.45 – 11.10 GHz)	39.35
Simulated F-RDRA	9.42 GHz 11.99 GHz	4.875 GHz (7.735 – 12.610 GHz)	47.92
Measured F-RDRA	7.62 GHz 12.3 GHz	6.048 GHz (7.0-13.048 GHz)	60.34

Table 5.3 Simulation results of the conventional DS-RDRA and the proposed F-RDRA.

DRA Shape	Frequency (GHz)	3-dB Beamwidth (degrees)		Gain (dB)
		E-plane	H-plane	
DS-RDRA	9.42	97	73	6.62
	11.99	65	1	6.02
F-RDRA	9.42	91	82	5.99
	11.99	82	14	6.48

Table 5.4 Parameters of DS-RDRA and proposed F-RDRA for theoretical analysis of antenna design.

Parameters	DS-RDRA	F-RDRA
L_d (length)	10 mm	8.69 mm (since curve shape at upper segment of RDRA therefore calculate average value of a considering total curve surface area as a trapezoidal)
W_d (width)	20 mm	20 mm
b ($2*(H_d+H_t)$)	(2.5+3.5)*2 = 12 mm	12 mm
ε_u (permittivity of upper segment)	15	15
ε_l (permittivity of lower segment)	2.1	2.1
d (height of upper segment)	2.5 mm	2.5 mm
t (height of lower segment)	3.5 mm	3.5 mm

For experimental demonstration, the F-RDRA was fabricated using the filleted BST-3P ceramic (ε_r = 15) as upper segment and Teflon (ε_r = 2.1) as lower segment of the proposed antenna. The aperture coupling with microstrip line feed was used to excite the proposed antenna. The experimental reflection coefficient versus frequency characteristic of the proposed F-RDRA is given in figure 5.3(c) along with its simulated characteristic. It can be seen from figure 5.3(c) that experimental -10 dB reflection coefficient bandwidth of 6.04 GHz (60%) for the proposed F-RDRA is obtained (The experimental bandwidth is also given in Table 5.2). The deviation in simulation and experimental results may be due to fabrication and measurement errors. The bandwidth parameters of single segment, conventional dual segment and the proposed F-RDRA extracted from

figure 5.3 are given in Table 5.2. From figure 5.3 and Table 5.2, it can be observed that F-RDRA provides the widest bandwidth among the antennas considered in the study. Table 5.5 shows the comparison of proposed antenna with existing antennas in the literature on the basis of different antenna parameters. It can be observed from Table 5.5 that proposed F-RDRA provides widest percentage bandwidth among existing antennas.

Table 5.5 Performance comparison of proposed antenna with other antennas reported in literature.

S.No.	DRA Shape	ε_d	Resonant Frequency (GHz)	Excitation	BW (GHz)	BW (%)	Ref.
1	Notched Rectangular shape	10.8	11.9	Slot coupling	10.1-13.7	28	Ittipiboon et al. (1996)
2	RDRA consisting of intermediate substrate.	2.2/10.2	12.3	Slot coupling	9.0-16.4	59	Coulibaly et al. (2006)
3	Rectangular	9.8	6.9, 9.7, 11.1, and 13.2	Parallel standing strips	-	60	Rashidian et al. (2012)
4	Proposed F-RDRA	2.1/15	7.62, 12.3	Aperture coupling	7.00-13.05	60.34	proposed

BW: Operating bandwidth

5.3.2 Mode analysis

The knowledge of different coupling mechanisms and the modes excited in antennas are required to get better understanding of antenna performance. While designing the dielectric resonator antenna, one should consider the mode generation and field distributions inside the resonating material. By properly combining one or more of the higher order modes with the fundamental mode, a wider bandwidth or dual- or multi-band operation can be achieved [Petosa (2007)]. In this section, the study of mode excitation is described for each RDRA considered in the present study. From field distributions shown in figure 5.4, $TE^{x}_{2\delta 1}$ mode is identified at resonant frequency of 11.32 GHz in SS-RDRA. Through the study of field distributions given in figure 5.5, it can be inferred that the

mode excited in upper segment of conventional DS-RDRA is $TE^{x}_{2\delta 2}$ mode (higher order mode) corresponding to resonant frequency of 8.68 GHz. In lower segment of the antenna, which works as an insert for the antenna, $TE^{x}_{2\delta 1}$ mode (lower order mode) corresponding to resonant frequency of 8.68 GHz is excited. Figure 5.6 shows the field distributions in upper and lower segments mode of the proposed F-RDRA. It is inferred through Figure 5.6 that the mode exited in upper segment of the proposed Filleted RDRA is pure TE^{x}_{211} mode corresponding to a resonant frequency of 9.42 GHz. The mode excited in lower segment of the Filleted antenna, which acts as an insert is TE^{x}_{2n1} corresponding to a resonant frequency of 9.42 GHz. The number 'n' in TE^{x}_{2n1} mode lies between δ and 1. The middle number 'n' in TE^{x}_{2n1} mode in the lower segment of antenna arises due to the fact that field variation along y-direction lies between a fraction of half cycle to full half cycle. Each mode of an antenna structure corresponds to a resonant frequency. Resultant field distribution may be modified due to change in modes or generation of more modes.

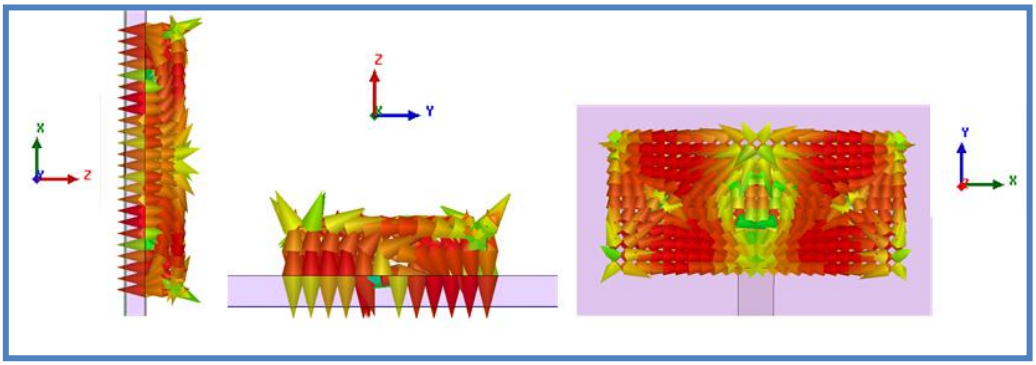

Figure 5.4 E–field distribution of SS-RDRA at 11.32 GHz.

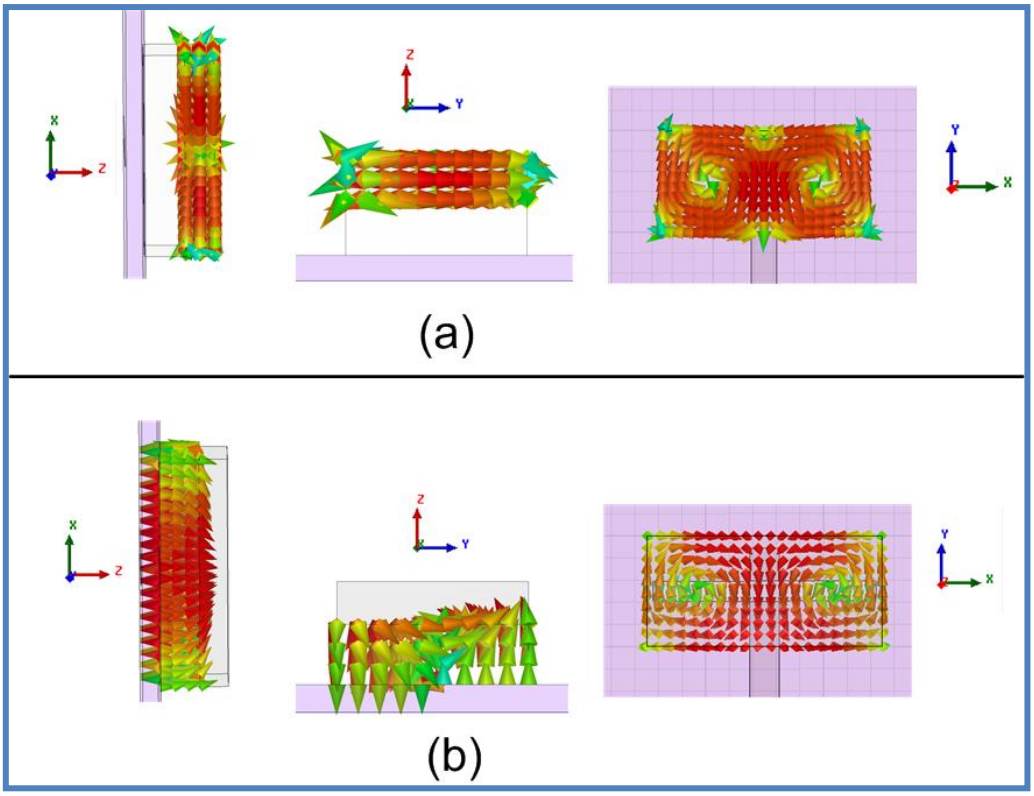

Figure 5.5 E–field distributions in DS-RDRA of (a) upper segment, and (b) lower segment at 8.68 GHz.

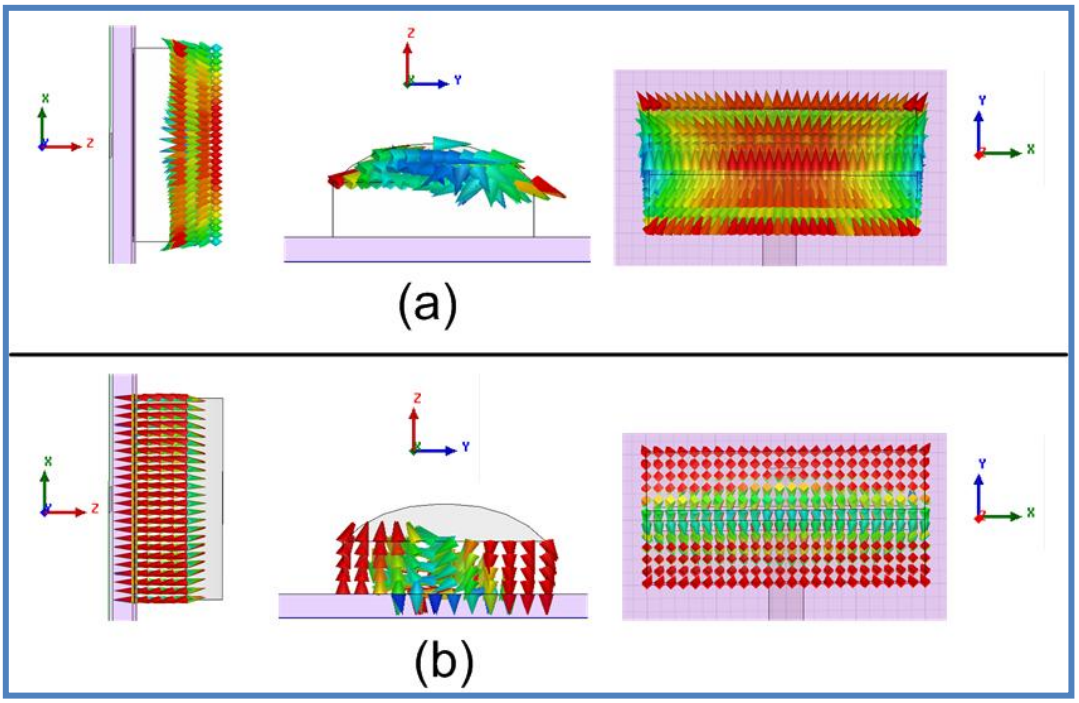

Figure 5.6 E–field distributions in F-RDRA of (a) upper segment, and (b) lower segment at 9.4 GHz.

5.3.3 Radiation patterns and gain of the proposed antenna

Figure 5.7 shows the simulated 3-dimentional radiation patterns of conventional DS-RDRA and proposed F-RDRA at the frequencies of 9.42 and 11.99 GHz. Further Fig. 5.8 shows the simulated 2D radiation patterns of the two antennas in H–plane at simulated resonant frequencies of the proposed F-RDRA. At lower frequency i.e. at 9.42 GHz, radiation patterns are stable for both the designs. As we move from lower to the higher frequencies (9.42 to 11.99 GHz), the radiation pattern of proposed F-RDRA remains nearly stable in terms of frequency. Due to more discontinuities in the conventional DS-RDRA, diffraction from the edges occurs which causes generation of ripples in radiation pattern. The edge diffraction increases when we move from lower to higher frequencies. In the proposed F-RDRA, number of discontinuities (edges) reduces resulting in stable radiation patterns at higher frequencies also.

Radiation pattern and gain measurement was performed in the anechoic chamber as shown in figure 3.8. Measurement setup consist of single VNA (Anritsu MS231C) used as source for test antenna as well as receiving display for DUT (Device under test). The gain of fabricated antenna was measured using Two antenna method, in which horn antenna with known gain was used as a test antenna.

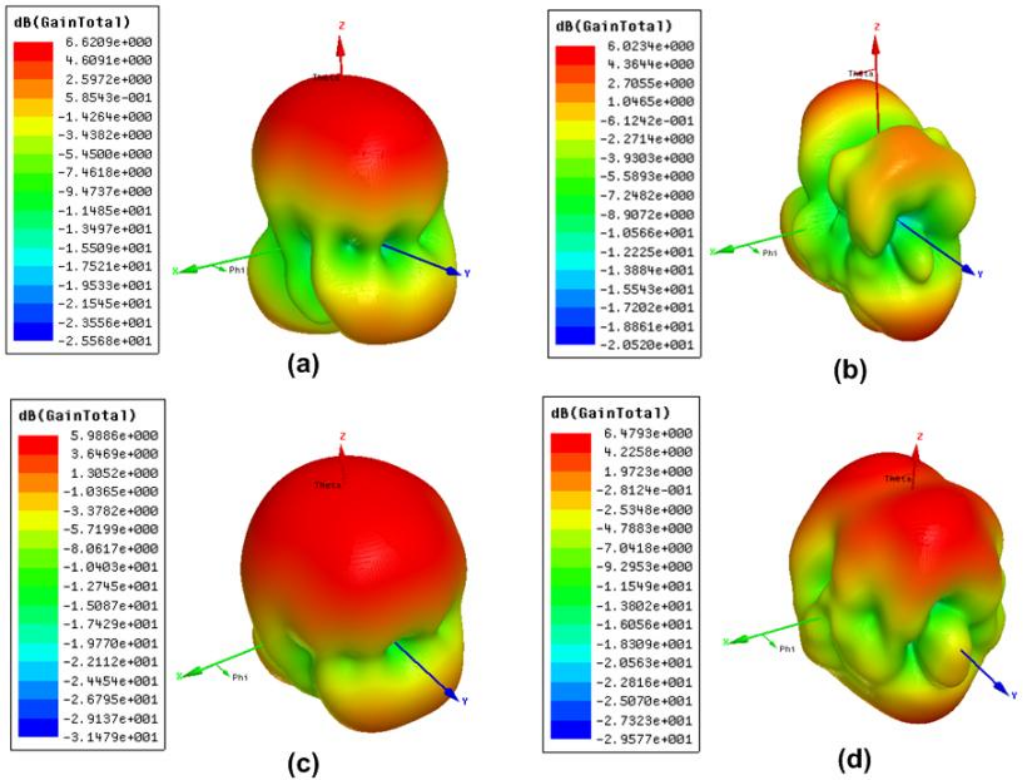

Figure 5.7 Simulated 3D radiation pattern of (a) Conventional DS-RDRA at 9.42 GHz; (b) Conventional DS-RDRA at 11.99 GHz; (c) F-RDRA at 9.42 GHz and (d) F-RDRA at 11.99 GHz.

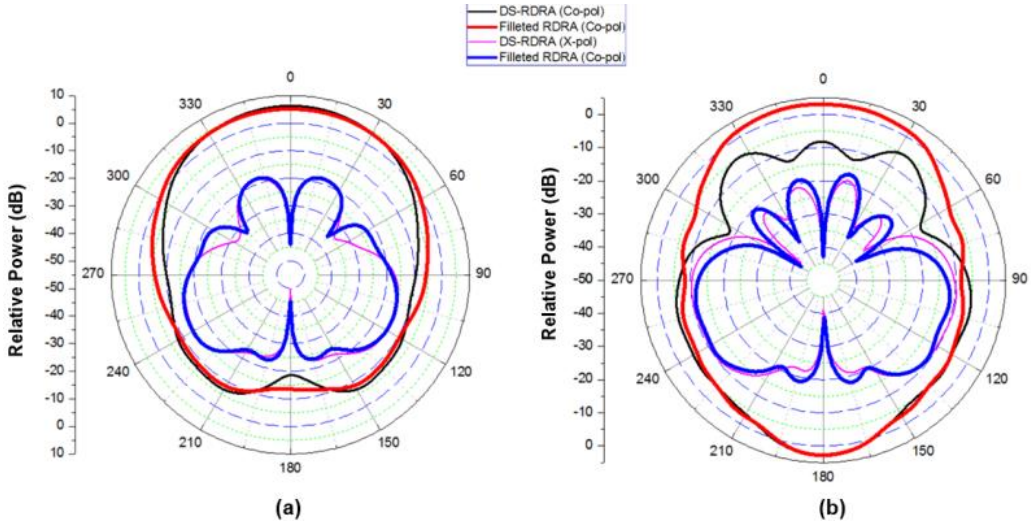

Figure 5.8 Simulated far field radiation pattern of conventional DS-RDRA and F-RDRA in H–plane at: (a) 9.42 GHz; (b) 11.99 GHz

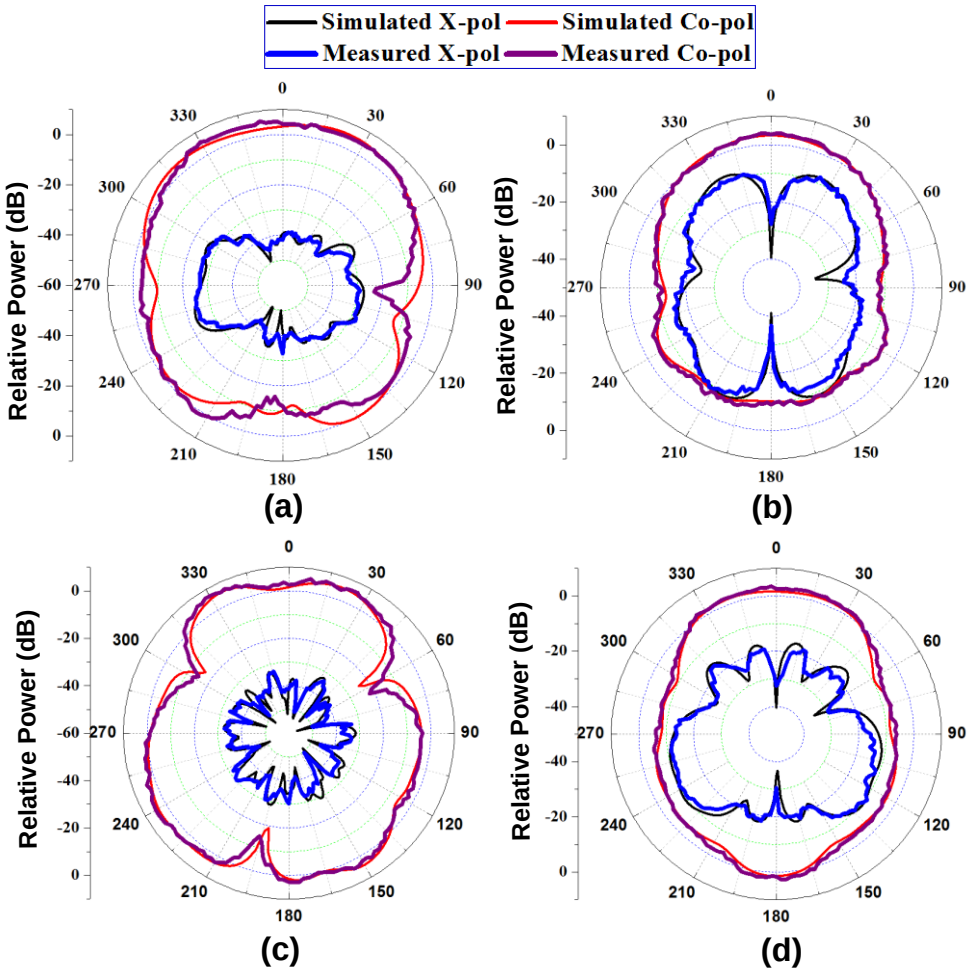

Figure 5.9 Far field radiation patterns of F-RDRA in :(a) E-plane at 7.62 GHz; (b) H-plane at 7.62 GHz; (c) E-plane at 12.3 GHz, and (d) H-plane at 12.3 GHz.

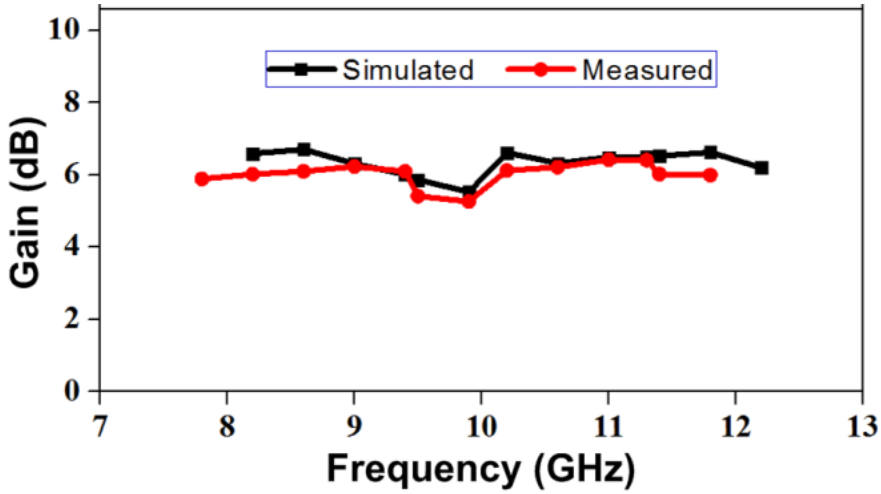

Figure 5.10 Simulated and measured gain values of F-RDRA over its operating frequency range.

Figure 5.9 shows simulated and measured 2D radiation patterns of F-RDRA in E– and H–planes at frequencies of 7.62 and 12.3 GHz (the measured resonant frequencies of the proposed F-RDRA). It can be seen from the figure 5.9 that simulated radiation patterns are nearly in agreement with corresponding experimental patterns.

The simulated 3dB beamwidths of conventional DS-RDRA and the F-RDRA at the resonant frequencies of the proposed F-RDRA are illustrated in Table 5.3. A comparison of E– and H–plane beamwidths of the two antennas reveals significant differences in the corresponding beamwidths of the antennas. The H–plane 3 dB beamwidth of the F-RDRA has increased by 9 degrees and E plane beamwidth has decreased by 6 degrees as compared with conventional DS-RDRA at a frequency of 9.42 GHz. But at higher resonant frequency of 11.99 GHz, both the E– and H–plane beamwidths have increased by higher amount in case of F-RDRA as compared with DS-RDRA. Thus, the distorted 3D radiation pattern at the higher resonant frequency observed in the case of DS-RDRA gets significantly improved in proposed F-RDRA due to significant increase in the 3dB bandwidths in both E– and H–planes of the proposed antenna. Figure 5.10 shows the variations of simulated and measured gain values of the proposed antenna over its operating frequency range of 7.73 - 12.61 GHz and 7.0 - 13.04 GHz respectively. The simulated and measured results are nearly in agreement with each other.

5.4 Summary

In the present chapter, prepared ceramic BST-3P has been used for the design, simulation and experimental studies on F-RDRA. The simulated -10 dB reflection coefficient bandwidth of the proposed antenna has been found to be 4.875 GHz, which is 8.57 %

greater than 3.65 GHz, the bandwidth of conventional dual segment RDRA. The experimental -10 dB reflection coefficient bandwidth of the fabricated F-RDRA is 6.048 GHz (7.00 – 13.048 GHz) with nearly 60% impedance bandwidth. The proposed F-RDRA provides widest bandwidth with reasonable gain among all the RDRAs studied and those reported in literature. The proposed F-RDRA provides broadside radiation pattern with reasonable good realized gain over its operating frequency range. The proposed antennas can find potential application as primary feed for parabolic reflector in radar and satellite communication.